ACS OMEGA

Open Access

http://pubs.acs.org/journal/acsodf

Article

Comparative Study of Single and Coaxial Electrospun Antimicrobial Cross-Linked Scaffolds Enriched with Aloe Vera: Characterization, Antimicrobial Activity, Drug Delivery, Cytotoxicity, and Cell Proliferation on Adipose Stem Cells and Human Skin Fibroblast

Damian Francisco Plascencia Martinez, Jesús Manuel Quiroz Castillo, Alida Ospina Orejarena, Alfonso Pérez Gallardo, Emilio Méndez Merino, Gerardo Asael Trimmer López, Itzel Yanira López Peña, Diego Hernández Martínez, Karla Alejandra López Gastelum, Abraham Alejandro Leyva Verduzco, Antonio S. Ledezma, and María Mónica Castillo Ortega*

Cite This: *ACS Omega* 2024, 9, 41157−41170

Read Online

ACCESS | Metrics & More | Article Recommendations

ABSTRACT: The preparation of materials with application in the biomedical field needs to attend some characteristics such as biocompatibility, nontoxicity, adequate mechanical properties, and the ability to mimic the extracellular matrix. Scaffolds for use in cell culture were prepared based on gelatin, polylactic acid (PLA), aloe vera mucilage, and tetracycline. Fibers were prepared in single and coaxial configuration and then cross-linked with glutaraldehyde saturated vapor. The fibers were obtained with cylindric morphology and changed to ribbon morphology and porous membranes, similarly to the extracellular matrix, when cross-linked. Membranes prepared by coaxial electrospinning showed core−shell structures when observed by transversal images, which is beneficial for controlled drug release. Characterization techniques such as scanning electron microscopy, thermogravimetric analysis, and Fourier transform infrared spectroscopy demonstrated the cross-linking due to the increase in diameter, formation of imine groups, and improvement of thermal stability. Antibiotic release tests showed that the prevalent release mechanism is diffusion and can be controlled considering the encapsulation effect, when fibers are prepared with a coaxial configuration, increasing the drug release time, making it a suitable material for controlled release. The biological evaluation of the scaffolds was carried out in two cell lines: mammalian adipose stem cells (ASCs), used as a primary cell culture, and Detroit 548 human skin fibroblasts as a dermal cell model. Aloe vera enriched scaffolds showed better activity in contact with both cell lines, exhibiting cell viability values greater than 90% and favorable results in live−dead assays when no damaged cells were observed. Cell proliferation was evaluated using Detroit 548 human skin fibroblast on gelatin-based scaffolds by the staining of the adhered cells; the images showed good confluence and morphology of the cells on the aloe vera and antibiotic loaded membranes for both of the studied configurations. Antibiotic loaded membranes presented antimicrobial activity against *S. aureus*, and this behavior increased when aloe vera is included. According to the results, the scaffolds prepared on single configuration enriched with aloe vera and tetracycline could be used in dermal tissue engineering as burn dressings, diabetic foot apposite, and skin substitutes, and the scaffolds prepared with a coaxial configuration are recommended for controlled release systems of antibiotics as treatments for chronic wounds such as diabetic foot and burn healing.

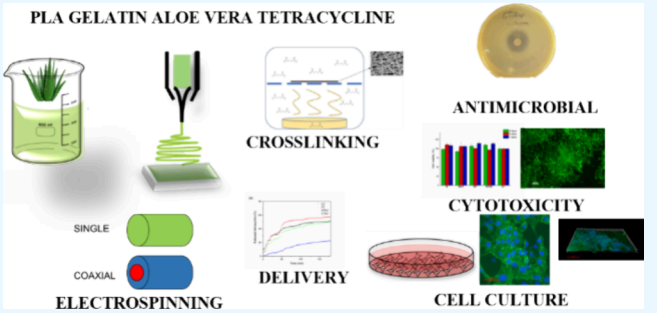

INTRODUCTION

The effective management of wounds requires the creation of an optimal microenvironment to facilitate proper healing. In this regard, wound dressings play a crucial role by providing a temporary physical barrier against bacterial contamination, promoting the required moisture for optimal re-epithelialization, and facilitating the correct absorption of wound exudate.[1−7]

In the case of nonhealing wounds like diabetic wounds, venous ulcers, and pressure ulcers effective wound healing is a challenging process due to delayed healing and risk of infection.[8−11] Conventional dressings such as gauzes and

Received: January 31, 2024
Revised: June 17, 2024
Accepted: June 19, 2024
Published: September 29, 2024

bandages prove insufficient in creating the required moist conditions but act as a support for more sophisticated dressings.[12,13] Moreover, the use of creams and gels is necessary to supply antibacterial substances. However, these topical applications typically carry a maximum drug load of 5%, requiring constant reapplication and contributing to additional pain due to manipulation of the wound.[14−19]

To address these issues, advances in wound dressing materials are crucial. Electrospun nanofiber meshes have emerged as a promising solution, offering advantages such as high surface area, porosity, and the ability to incorporate drugs.[20−26]

The method of electrospinning has become incredibly promising, particularly in the field of clinical applications. Its popularity is attributed to its simplicity, cost-effectiveness, and scalability, which are all critical characteristics to produce materials for clinical use.[27−29] The principle of electrospinning requires the use of an electric field to create thin polymer fibers. A solution of a prepolymer and a solvent is placed into a syringe and subjected to a high electric field, which induces the formation of a cone-shaped droplet at the syringe tip. From this cone, a jet of liquid is propelled outward. As this jet travels through the air, the solvent within it evaporates, leaving behind a charged polymer fiber. These fibers are collected to form a nonwoven fabric, by adjusting parameters like electric field power, type of collector, temperature, humidity, the use of coaxial needles, and polymer concentration.[30] Fibers can be tailored for specific applications, making electrospinning a versatile tool in fields like tissue engineering and drug delivery.[31−34] Coaxial electrospinning is obtained when two concentric needles are used to generate core−shell fibers and has gained attention in drug delivery applications for the controlled release of active compounds. The significant contribution of the coaxial structure to the controlled release of active compounds is to be able to modulate the release of the active components. As is known, if the active component is in the center of the fibers, the outer layer acts as protection for bioactive components making it suitable for controlled release applications.[35,36]

Gelatin is a biopolymer of natural origin that presents high biodegradability, biocompatibility, and water absorption and is available commercially. Gelatin has been widely used in various forms and has been successfully electrospun into membranes and tested on biomedical applications as drug delivery and wound dressing.[37−40] Polylactic acid (PLA) is a biocompatible polyester, which use in different biomedical applications has been approved by the FDA and is widely used in surgery and traumatology.[41,42] The combination of gelatin and PLA has been proposed as a biocompatible material. Nanofibers prepared in a coaxial configuration using these two polymers with gelatin in the core, containing the active compounds, and PLA in the shell, conferring the structure and mechanical properties, would serve as potential materials for wound dressing and tissue engineering applications.[43,44]

The use of conventional antibiotics has not yet been replaced in applications where there is a high microbial load, such as the treatment of burns and the diabetic foot. Tetracycline is a broad-spectrum antibiotic that has been incorporated into electrospun fibers; it has been shown that the activity of this antibiotic remains after its incorporation.[45,46] Aloe vera is a plant well-known for its potential therapeutic action; numerous benefits have been attributed to it, including immunomodulation and healing of wounds and burns. The part of the plant that presents these activities is the mucilage, which is a viscous substance, like rubber, that is found inside the leaves. Plant-derived carbohydrates have exhibited diverse biological activities.[47−51]

In this article, we present an investigation of the potential use of electrospun membranes prepared by coaxial electrospinning as a promising material for skin dressing applications. Our study focuses on addressing the limitations of conventional dressings by creating a novel material by the electrospinning technique, which includes a conventional antibiotic to prevent the wound from bacterial infection and a bioactive natural compound like aloe vera mucilage that would enhance cell proliferation and tissue repair. Through comprehensive experimental characterization and evaluation of cell viability, we seek to demonstrate the potential of these membranes as advanced wound dressings with enhanced properties for healing applications, such as diabetic foot treatments and burn healing.

MATERIALS AND METHODS

Materials. Gelatin from porcine skin, gel strength 300 type A, tetracycline hydrochloride, and glacial acetic acid, ACS reagent, were supplied by Sigma-Aldrich. PLA 4060D, Mw= 119000 g mol^{-1} was supplied by NatureWorks. Glutaraldehyde, 25% aqueous solution, was supplied by Merck. Calcein-AM, ethidium homodimer, and Presto Blue were supplied by Invitrogen. Acetone was supplied by Fagalab. Phalloidin-Alexa Fluor 488 and Hoechst 33342 were supplied by Thermofisher Scientific. Aloe vera leaves were locally collected in Hermosillo, Sonora, Mexico (29°04′30″N 110°57′30″O).

Extraction of Aloe Vera Mucilage (Av). Extraction of mucilage from aloe vera was adapted from Medina-Torres et al.[52] as follows: aloe vera leaves with a healthy appearance were collected. The external part of the leaf was removed, and the inner gel was semifrozen and processed into a blender. The juice obtained from this process was filtered and centrifuged at 15000 rpm for 30 min to eliminate bigger solids. Supernatant was frozen and then freeze-dried for 4 days. The obtained material was minced, resulting in aloe vera powder.

Membrane Preparation. Membranes were prepared by electrospinning. Gelatin solution at 20% (w/v) was prepared by dissolving the biopolymer into an acetic acid aqueous solution (90%). PLA was dissolved in acetone at a concentration of 10% (w/v). Aloe vera mucilage (Av) or tetracycline (T) was added into gelatin loaded solutions by adding the respective compound in the polymeric solution at 1% (w/v). A summary of the obtained membranes is listed on Table 1.

Table 1. Component Concentration on Polymeric Electrospun Mats[a]

system	arrangement	gelatin % (w/v)	PLA % (w/v)	aloe vera mucilage % (w/v)	tetracycline hydrochloride % (w/v)
S1	single	20			
S2	single	20		1	
S3	single	20			1
S4	single	20		1	1
S5	single		10		
S6	single		10		1
C1	coaxial	20	10		
C2	coaxial	20	10	1	
C3	coaxial	20	10	1	1

[a]Coaxial configuration fibers were prepared using PLA solution as the shell and gelatin as the core. Active compounds were dissolved on the gelatin solution.

https://doi.org/10.1021/acsomega.4c01016
ACS Omega 2024, 9, 41157−41170

Polymeric solutions were set into 6 mL syringes and placed in a KDS Scientific peristaltic pump with a flow rate of 1 mL h^{-1}. Voltage of 15 kV was supplied using a Spellman CZE 1000R power supply, and the distance between the needle and the collector was 15 cm. An aluminum plate (10 × 10 cm) was used as collector. Coaxial configuration fibers were prepared using PLA solution as the shell and gelatin as the core with a flow rate of 0.5 mL h^{-1} for each solution (1 mL h^{-1} total).

For improvement of the stability of the obtained gelatin-based membranes and prevention of dissolution in aqueous media, it was decided to cross-link. For cross-linking, a 25% glutaraldehyde solution was employed, using the saturated vapor method. Membranes obtained by electrospinning technique were dried at room temperature to eliminate the remaining solvent and then placed in a cross-linking chamber with 1 mL of glutaraldehyde and sealed. After 48 h, cross-linking membranes were placed in an oven at 35 °C for 48 h to eliminate glutaraldehyde excess.

Characterization. Membranes obtained from single systems were morphologically characterized by scanning electronic microscopy using a JEOL 5410LV microscope. An electron beam of 15 kV intensity was used at high vacuum; the samples were coated with a gold film. Coaxial configuration membranes were analyzed using a JEOL JSM-7401F, and samples were gold−palladium sputter-coated and measured using an electron beam of 2 kV with a secondary electron detector. Transversal images of coaxial fibers were measured to show the core−shell structure. Diameter distribution of fibers was measured using ImageJ software; at least 50 measurements of each system were performed. Transmission electron microscopy was used to determine the coaxial core−shell arrangement of the coaxial fibers. This analysis was performed with a transmission electron microscope JEOL 2010F, with an accelerating voltage of 200 kV. The samples were collected directly from the aluminum plate and placed in a copper mesh grid for the analysis.

FTIR spectroscopy was executed to confirm the presence and interaction of the components in each system, a Frontier PerkinElmer infrared spectrophotometer was used with the additament for ATR measurements in a range from 4000 to 500 cm^{-1}, and 16 scans and a resolution of 1 cm^{-1} were set.

Thermogravimetric analysis (TGA) was obtained with a PerkinElmer Pyris 1 TGA apparatus. Samples (2−4 mg) were weighed and heated from 25 to 800 °C in a N_2 atmosphere with a heating rate of 10 °C min^{-1}.

Drug Delivery. Evaluation of the drug delivery capacity from the electrospun mats was conducted to determine the kinetics and mechanism release from single and coaxial systems. Membranes were placed in a 3 mL quartz cuvette with phosphate-buffered saline (PBS, pH 7.4) as release medium at a constant temperature of 37 °C. Samples were placed on a PerkinElmer Lambda 20 UV−vis spectrophotometer, and the absorbance of the solutions was measured every minute until equilibrium was reached, using a wavelength of 278.89 nm for aloe vera mucilage and 330 nm for tetracycline.

To obtain release kinetics, absorbance was plotted against time. These values were interpolated into a calibration curve previously made to determine the amount of drug released into the medium. To obtain calibration curves, 10 solutions of known concentrations (from 0 to 10 mg/dL) of the active compounds were measured. With these data, an adjustment was made to the following release models: Peppas (eq 1), Higuchi (eq 2), and zero order (eq 3) to find the release mechanism, taking the data below 60% of the release.

$$\frac{M_t}{M_\infty} = K_p t^n \tag{1}$$

$$\frac{M_t}{M_\infty} = kt^{0.5} \tag{2}$$

$$\frac{M_t}{M_\infty} = kt \tag{3}$$

where M_t is the amount of drug released at time t, M_∞ is the released drug in equilibrium, t is the time, n is the releasing coefficient, K_p is the Peppas coefficient, and k is the kinetic constant.

Antibacterial Activity. *Staphylococcus aureus* were first activated in a brain heart infusion (BHI) broth (DIFCO, USA), for 24 h at 37 °C. The well diffusion agar test was done according to the method by Ngamsurach and Praipipat and Vásquez-López et al.[53,54] The bacteria were washed with PBS and centrifuged for 15 min at 3000 rpm. Then, the *S. aureus* pellet was resuspended in PBS until it reached a final concentration of 1×10^5 CFU mL^{-1} (determined from the optical density at 600 nm). Bacterial suspension was used to inoculate BHI soft agar in a 1:10 v/v relation and placed in 60 mm Petri dishes. Once the agar gelatinated, each membrane was placed in the center of it. Bacterial growth inhibition zones were measured after 24 h of incubation at 37 °C. To measure the inhibition zone, pictures of each experiment were taken and processed with ImageJ software. Images were processed by taking cross sections between the sample and the inhibition zone on each experiment. Experiments were performed in triplicate, and inhibition halo is reported as the average value and its standard deviation for each sample.

Cell Culture. Mammalian adipose stem cells (ASCs) sample was obtained by the Sigma Alimentos Biotechnology Laboratory according to standard protocols, donated to carry out this study, and used on passage 3. Human skin fibroblast line Detroit 548 CCL-116 was supplied by ATCC and used on passage 8. Cells were grown in treated culture dishes ($D \times H$ 60 × 15 mm, Corning) at 37 °C and 5% CO_2 in Dulbecco's Modified Eagle's Medium (DMEM, Gibco) supplemented with 10% Fetal Bovine Serum (Biowest) and 1% Anti-Anti 100× (Gibco).

When a confluent growth was reached, cells were detached with 0.125% trypsin-EDTA (Gibco) for 4 min. Cell suspension was centrifuged (4 min, 1000 rpm), supernatant was separated, and cells were resuspended in fresh culture medium.

Cytotoxicity assay was performed in direct contact with the materials: membranes were cut into 7 mm diameter discs, sterilized by UV radiation (4 cycles, 15 min per side), and then sited in 96 well plates, seeding a total of 2.5×10^3 cells per well and incubated, and viability test was carried by triplicate at 3, 5, and 7 days of incubation using Presto-Blue (Invitrogen) reagent.

Measurements of cell viability were performed as follows: after 3, 5, and 7 days of incubation, the culture medium was removed and replaced by 200 μL of Presto-Blue enriched medium prepared as the manufacturer's instructions and incubated at 37 °C in the dark. Then, 100 μL of the test medium was placed on a 96 well plate. Absorbance was measured at 570 and 600 nm in a Multiskan Sky microplate reader (Thermoscientific).

Cell viability was obtained from the following equation:

https://doi.org/10.1021/acsomega.4c01016
ACS Omega 2024, 9, 41157−41170

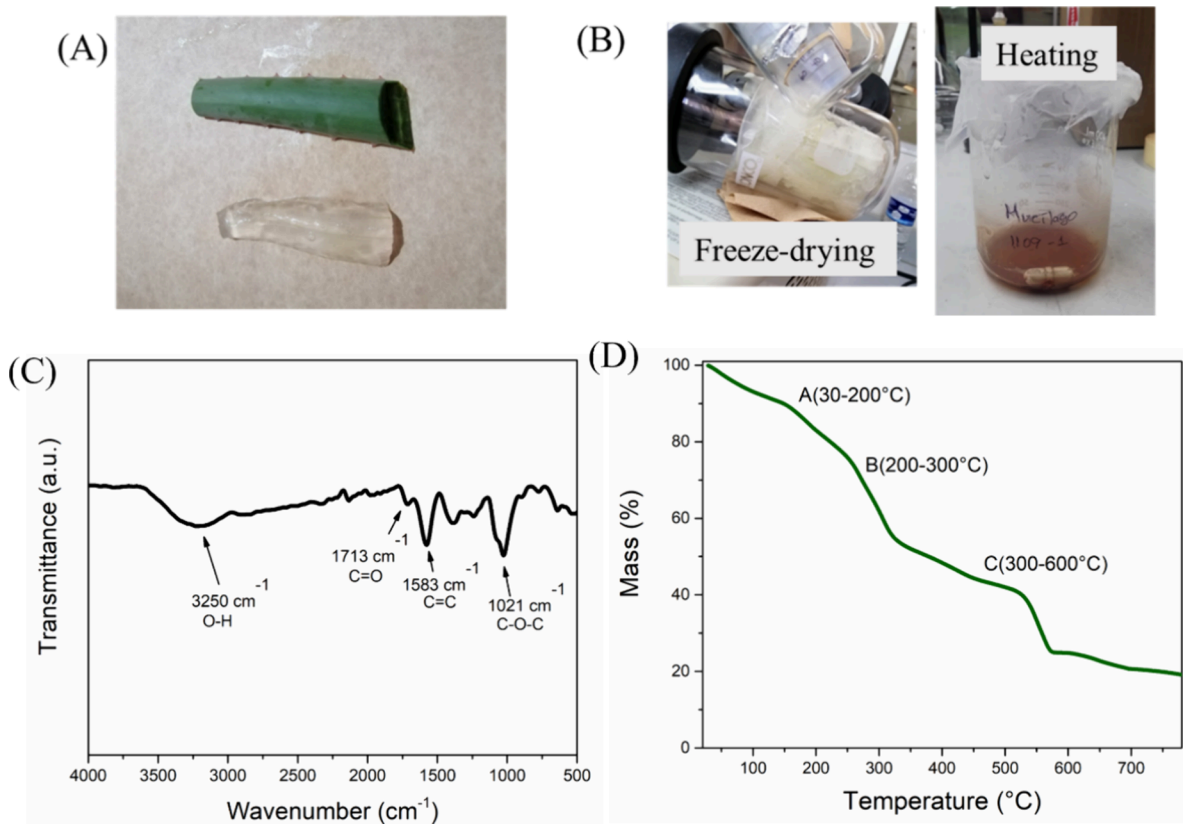

Figure 1. Aloe vera mucilage extraction and characterization. (A) Aloe vera leaf (up) and gel (down), (B) effect of drying process for aloe vera: freeze-drying (left) and heating (right), (C) FTIR spectra, and (D) TGA analysis.

$$\text{cell viability} = \left(\frac{(\varepsilon_{600} \times A_{570}) - (\varepsilon_{570} \times A_{600})}{(\varepsilon_{600} \times C_{570}) - (\varepsilon_{570} \times C_{600})} \right) \times 100 \quad (4)$$

where ε is the molar extinction coefficient, A is the absorbance of the sample, and C is the absorbance of the cellular control.

Live/Dead Assay. Cell viability of the polymeric scaffolds has been investigated by a Live/Dead assay on ASCs and Detroit 548 fibroblast. Cells were seeded on a concentration of 1×10^4 cells per well above the scaffolds in 24 well plates and cultured for 7 days. After this time, culture media was taken off and washed with PBS (pH = 7.4) solution, then 200 μL of solution of Calcein-Ethidium homodimer (Invitrogen) was added and incubated for 30 min at room temperature. The images were taken using an Eclipse Ti2E Nikon fluorescent microscope with excitations of 470 nm for calcein and 560 nm for Ethidium homodimer fluorescence, and an overlay image was formed from mixing both fluorescent channels.

Cell Proliferation. Cell proliferation assay of Detroit 548 fibroblast was performed from the cell staining on cultured membranes that contained gelatin, single systems (S1−S4), and coaxial systems (C1−C3). First, scaffolds were cut onto 1 cm × 1 cm squares, sterilized by UV, and placed on 24 well plates. Mats were seeded with Detroit 548 fibroblast on passage 8 with concentration of 1×10^4 cells per well and cultured for 7 days. Cells were fixed at days 3, 5, and 7 of culture by addition of 4% *p*-formaldehyde solution (w/v) for 20 min. After fixation, 0.01% Triton-X (Sigma-Aldrich) was added for 15 min, washed three times with PBS, and blocked for 30 min with 0.1% Bovine Serum Albumin (Sigma-Aldrich), and then, Phalloidin-Alexa 488 (1:400) was added and incubated for 1 h; after that, it was washed with PBS and Hoechst solution (Invitrogen) was added for 20 min. The images were taken using an Eclipse Ti2E Nikon fluorescence microscope with excitations of 385 nm for Hoechst and 470 nm for Phalloidin-Alexa 488 complex fluorescence. Cell proliferation was evaluated as the progression of cell confluence from the nucleus (blue channel), the morphology of the cells, and the formation of ECM from the actin staining (green channel).

RESULTS AND DISCUSSION

Aloe Vera Mucilage Obtention. To obtain mucilage, native aloe vera leaves with a healthy appearance were selected, that is, a green surface without the presence of brown spots, such as those presented in Figure 1A, and then, the external part of the leaf was separated into in its entirety, leaving the gel exposed, which was washed with deionized water and stored for later use.

The use of bioactive materials of natural origin requires adequate processing since during handling, they are susceptible to losing biological activity due to treatment. According to different authors such as Ramachandra and Rao,[55] one of the treatments that best preserves the characteristics of aloe vera gel is freeze-drying. The left side of Figure 1B shows the freeze-drying of the mucilage recovered after the extraction process. It can be seen that the sample retains its white color with slight shades of green and yellow. On the contrary, when it was dried with heat, the mucilage changed toward reddish and brown tones as shown in the right side of Figure 1B. This color change can be attributed to the oxidation of the components present in the gel, as pointed out by Baghersad et al.,[56] where it is indicated that it may be due to both atmospheric oxidation and bacterial

https://doi.org/10.1021/acsomega.4c01016
ACS Omega 2024, 9, 41157−41170

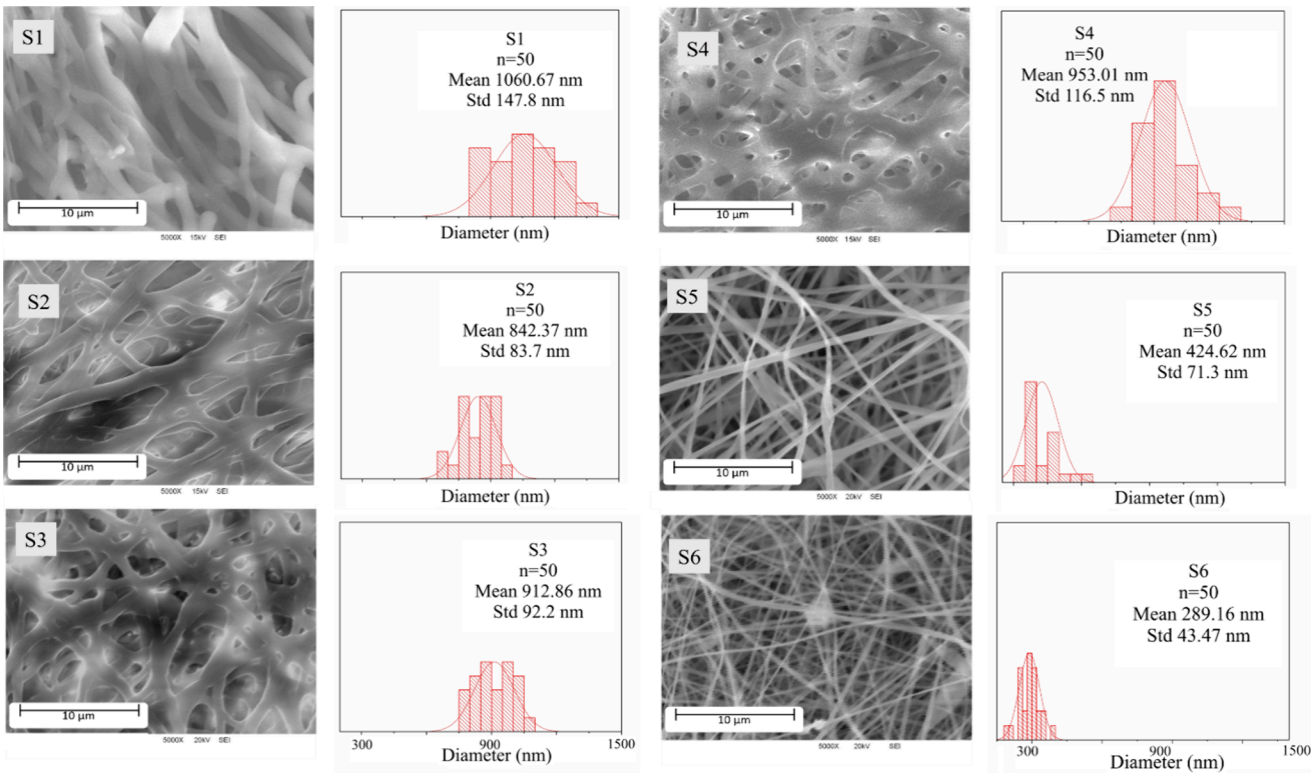

Figure 2. SEM micrographs at 5000× (left) and diameter distribution in the range of 300−1500 nm (right) of electrospun membranes prepared on single configuration.

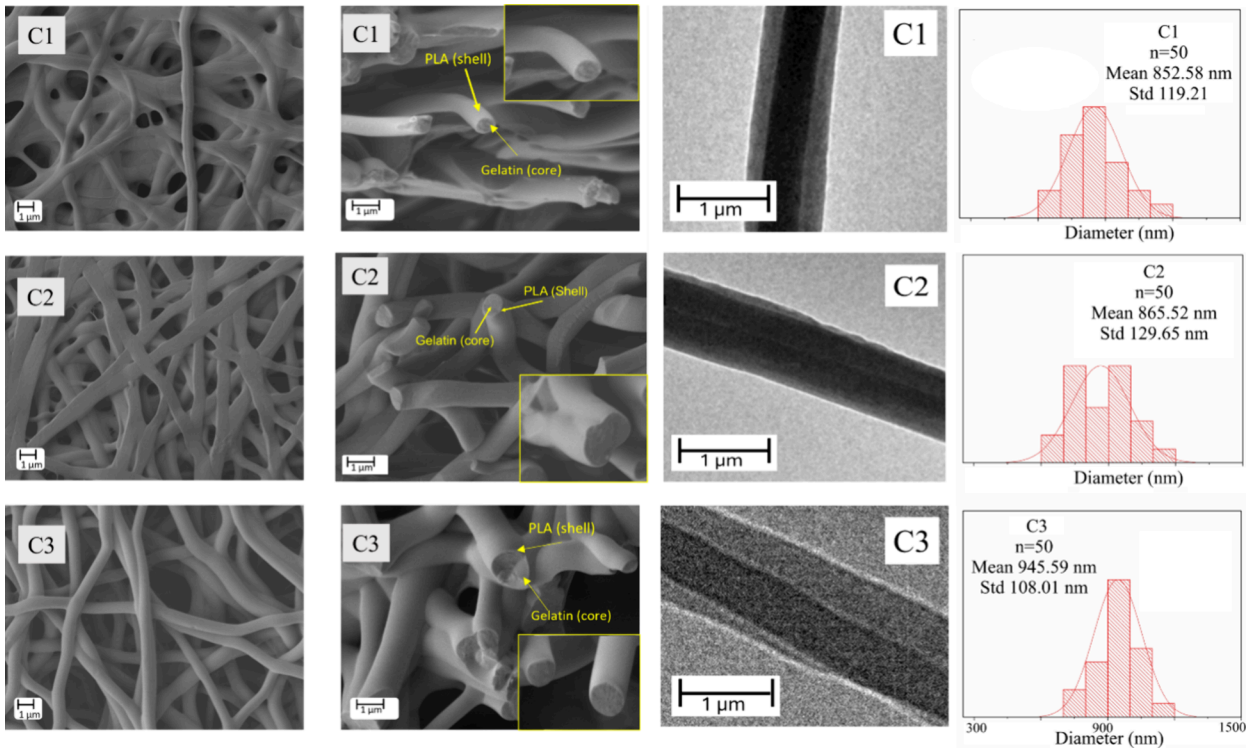

Figure 3. SEM micrographs at 5000× (left), transversal images at 10000× of coaxial electrospun fibers and TEM micrographs of coaxial fibers (center), and diameter distribution in the range of 300−1500 nm of electrospun membranes prepared on coaxial configuration (right).

growth and subsequent enzymatic degradation, which is why freeze-drying is chosen to dry this material.

The FTIR spectrum of aloe vera mucilage is shown in Figure 1C. Several signals can be identified, at 3250 cm^{-1}, a band corresponding to the O−H stretching appears, and other signals at 1713, 1583, and 1021 cm^{-1}, corresponding to C═O, C═C and C−O−C bonds, respectively. This analysis agrees with the composition reported by Abbasi et al.,[57] who attribute these

https://doi.org/10.1021/acsomega.4c01016
ACS Omega 2024, 9, 41157−41170

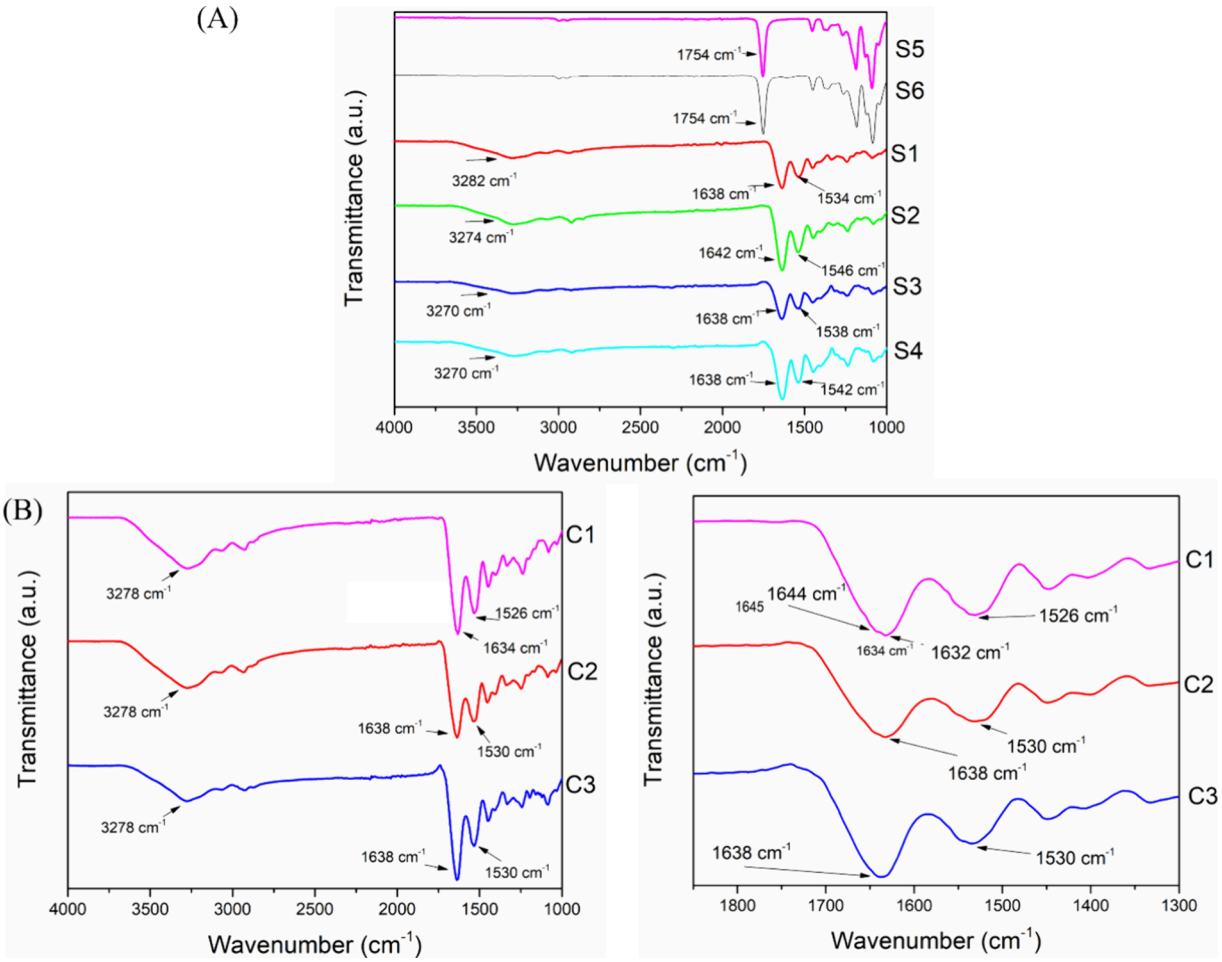

Figure 4. Fourier transformed infrared spectra (FTIR) of electrospun membranes prepared on (A) single configuration (S1−S6) and (B) coaxial configuration (C1−C3), right side is a close-up of the FTIR in the range of 1800−1300 cm^{-1}.

signals to the medicinal components of the plant such as phenolic compounds and polysaccharides.

An important aspect in the characterization of materials is their thermal stability; thermogravimetric analysis gives information on the behavior of the material when heated in a controlled atmosphere. Figure 1D shows the thermogram of a sample of lyophilized aloe vera gel; three degradation steps can be observed, which tells us about the varied nature of the gel. Before 200 °C, on step A around 10% of mass is lost, which can be attributed to the remaining moisture in the material, while between 200 and 300 °C, around 10% of mass is lost in step B, which can be attributed to low molecular compounds as flavonoids and galactomannans. On the other step, pointed as C, between 300 and 600 °C the degradation corresponds to the organic compounds such as polysaccharides and proteins.[58] After 800 °C is reached, there is a remainder of around 19%, corresponding to ash. This value can be compared to what was reported by Femenia et al.,[59] in their study report 23.6% as the ash content present in aloe vera gel, a value close to the 19% found by this analysis.

Membrane Obtention and Physicochemical Characterization. *Morphology.* The cross-linking of gelatin prevents its dissolution in physiological media. Various methods have been reported, both physical and chemical; the glutaraldehyde saturated vapor method was chosen since it allows the shape of the fibers to be preserved.[60] Both physical and chemical characteristics of the cross-linked materials changed due to treatment. SEM micrographs of fibers prepared on single configuration are shown in Figure 2. Pure gelatin fibers exhibit a rounded morphology, and after cross-linking reaction is performed, it acquires a morphology of ribbons, due to interactions between gelatin amine groups across the fibers when glutaraldehyde is incorporated. Pure gelatin cross-linked fibers (S1) present a diameter of 1060 nm, and enriched fibers present diameters of 823, 919, and 966 nm for S2, S3, and S4, respectively, and ribbon compact morphology. Pure PLA fibers (S5) show a diameter of 424 nm, while the antibiotic loaded PLA fibers (S6) diameter decreased to 289 nm. The diameter distribution on single electrospun fibers is presented on the right side of the Figure 2. The incorporation of active compounds led to more uniform fibers in comparison to uncharged fibers, as can be seen when comparing the distribution and standard deviations from S1 to S2, S3 and S4, and S5 to S6.

SEM micrographs of the membranes prepared in coaxial configuration are presented on the left part of Figure 3. The diameter of the fibers is 832, 865, and 945 nm for C1, C2, and C3, respectively. In comparison with membranes prepared on single configuration, the diameter is lower than gelatin membranes due to presence of PLA on the shell of the fibers, as PLA fibers have lower diameters but the ribbon like morphology appears after the cross-linking reaction. The center columns of Figure 3 show transversal cuts of fibers and TEM images to evidence the inner structure of membranes prepared in a coaxial configuration, displaying the core−shell structure of

https://doi.org/10.1021/acsomega.4c01016
ACS Omega 2024, 9, 41157−41170

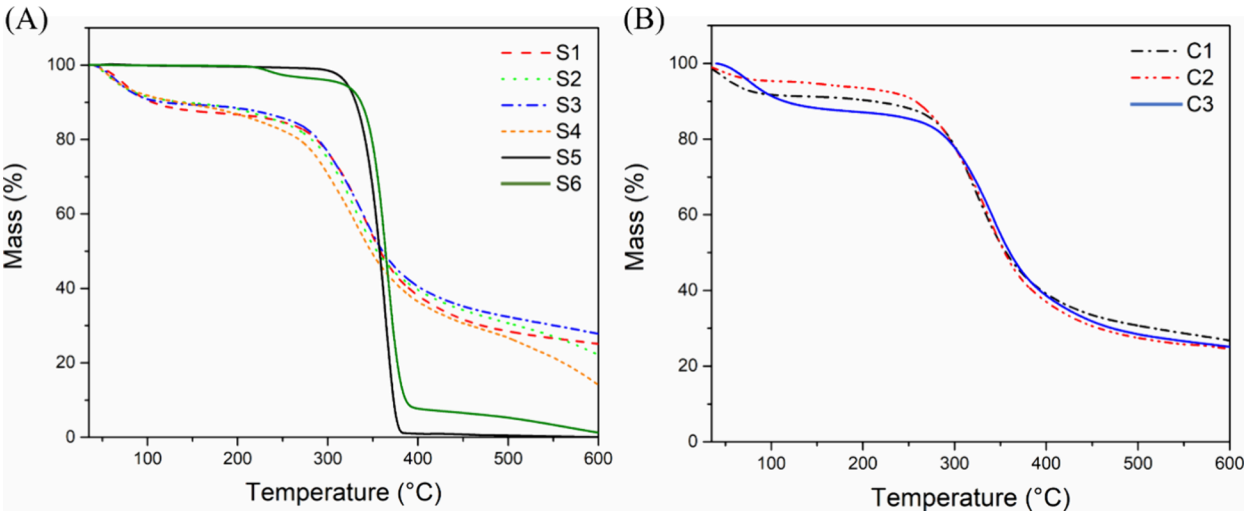

Figure 5. TGA thermograms of prepared membranes on (A) single configuration and (B) coaxial configuration.

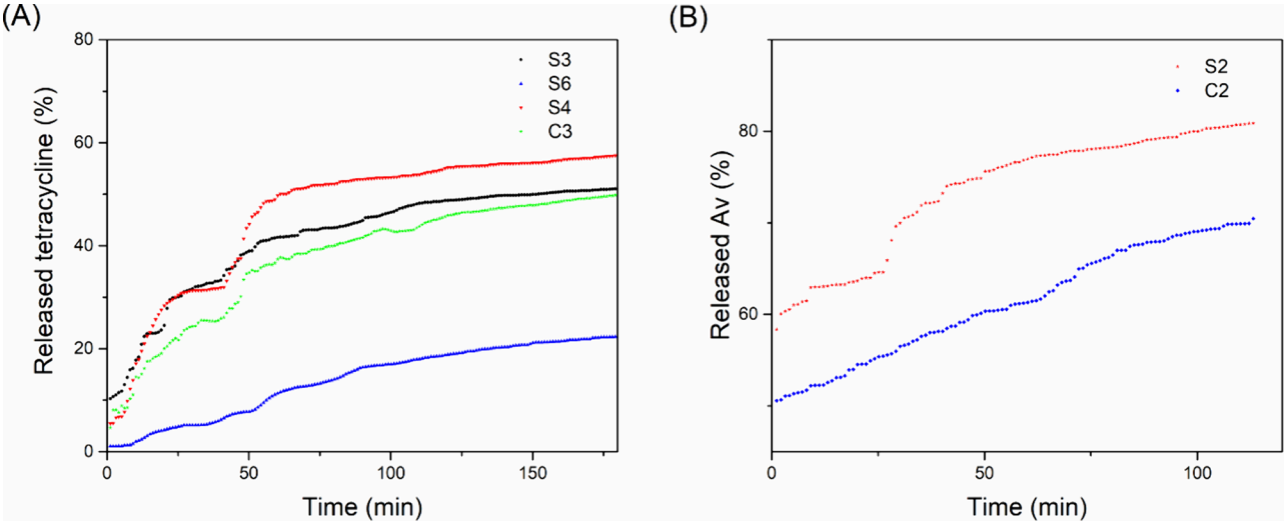

Figure 6. Drug release kinetics of (A) tetracycline and (B) aloe vera from electrospun membranes prepared on single and coaxial configurations. Release performed on PBS (pH 7.4) at 37 °C.

the fibers. The inner part is formed by gelatin and active compounds and the outer part by PLA, providing a protective layer on the material, which could enhance the controlled release properties. On the right side of Figure 3, the diameter distribution of the fibers prepared in the coaxial configurations is presented. As on single configuration fibers, the size distribution is affected by the addition of active compounds.

Both single and coaxial fibers exhibit porous membranes like the extracellular matrix, which is recommended for tissue engineering applications.[61,62] Changes in the diameter of loaded fibers, as well as the size distribution, are attributed to changes on the charges of polymeric solution when the electrospinning process is being performed.

Physicochemical Characterization. FTIR spectra of the prepared membranes are shown in Figure 4. PLA fibers show signals at 1754 and 1452 cm^{-1} corresponding to C═O and C−H methylene scissoring peak, respectively. Figure 4A shows the FTIR spectra of cross-linked scaffolds prepared in single configuration. Cross-linking of gelatin with glutaraldehyde occurs from the interaction between the amino groups of gelatin and aldehyde, resulting in the incorporation of the cross-linker between gelatin chains and the formation of imine group.[60] The reaction can be evidenced by the decrease in the intensity of the band around 3200−3500 cm^{-1}, which can be explained by the insolubility and hydrophobicity of the cross-linked scaffolds, as well as a slight change in the signal attributed to the amide I group, which is was found at a wavenumber of 1639 cm^{-1} for the pure gelatin membrane, and with the signal for the cross-linked membranes at 1638 cm^{-1} for S1, S3, S4, and 1642 cm^{-1} for S2 membranes, which suggests cross-linking between the gelatin units, reducing the number of amine and carbonyl groups that reacted to form imine groups. FTIR spectra for membranes prepared on coaxial configuration are shown in Figure 4B, and unloaded fibers present a signal at 3278 cm^{-1} for O−H stretching and signals at 1634 and 1526 cm^{-1} for amide I and amide II, respectively, while on C2 and C3 peaks are found at 3278, 1638, and 1530 cm^{-1} for O−H stretching, amide I, and amide II, respectively. On the right side of Figure 4B, there is a close-up of the FTIR spectra in the area from 1800 to 1300 cm^{-1} for the coaxial systems. It can be seen in C1 that the main signal presents a shoulder at 1645 cm^{-1} due to the contribution of the carbonyl peak of PLA, while for C2 and C3, this peak is wider

https://doi.org/10.1021/acsomega.4c01016
ACS Omega 2024, 9, 41157−41170

Table 2. Drug Release Data from Electrospun Mats and Model Fitting to Drug Release Mechanism

system	released component	equilibrium time (min)	percentage of release (%)	model	R^2	model parameters		release mechanism
S3	tetracycline	130	50	zero order	0.9732	k	0.0171	diffusion
				Higuchi	0.9519	k	0.1118	
				Peppas	0.8892	n	0.5053	
						K_P	0.1128	
S4	tetracycline	150	58	zero order	0.8249	k	0.012	diffusion
				Higuchi	0.9159	k	0.1041	
				Peppas	0.9741	n	0.5952	
						K_P	0.0809	
C3	tetracycline	140	47.5	zero order	0.9255	k	0.0098	diffusion
				Higuchi	0.9754	k	0.0863	
				Peppas	0.9761	n	0.471	
						K_P	0.0977	
S2	AV	100	80	zero order	0.8771	k	0.0024	slow diffusion
				Higuchi	0.9451	k	0.0325	
				Peppas	0.9066	n	0.0344	
						K_P	0.7138	
C2	AV	100	70	zero order	0.9914	k	0.0027	slow diffusion
				Higuchi	0.969	k	0.0035	
				Peppas	0.983	n	0.0856	
						K_P	0.5961	

due to the overlap of these two peaks and the interaction of the active components. Changes in the peaks can be attributed from interaction between the components and the active compounds as well as the configuration of the membranes.

Figure 5 presents the thermogravimetric analysis of the prepared membranes. The thermal stability of gelatin-based membranes on a single configuration has changed due to incorporation of glutaraldehyde and active compounds. The temperature of highest rate of degradation was obtained from first derivative mass loss curve (DTG), resulting in 340, 331, 339, and 336 °C for S1, S2, S3, and S4 membranes, respectively. Higher values of degradation temperature show better thermal stability, which is attributed to the reaction with glutaraldehyde, but it decreases when active compounds are added to the fibers. For S5 fibers, a single-step degradation process can be seen with a temperature of the highest rate of degradation of 355 °C (obtained by DTG curve), while the S6 membranes show a two-step degradation, with two temperatures of degradation, one at 275 °C where approximately 5% of the mass is lost, attributed to the antibiotic, and the other at 360 °C where the remaining mass is lost, attributed to the matrix content. Membranes prepared in coaxial configuration present a three-step degradation, first the mass loss around 100−200 °C, attributed to moisture content on the membranes, then a second step at 330 °C, which can be assigned to the mass loss from the gelatin in the core, and a third step at 360 °C due to the loss of PLA on the shell of the membranes.

Drug Release. The discharge evaluations of the active agents from the membranes (aloe vera mucilage or tetracycline) were carried out using saline phosphate buffer medium (PBS, pH 7.4) and a temperature of 37 °C to mimic the body environment. Figure 6A shows the release kinetics of tetracycline from four different polymeric matrices, and similar release profiles were observed. The gelatin membrane with tetracycline (S3) presented a burst release of 16%, followed by a sustained release until 130 min, where it reached equilibrium after releasing 50% of the tetracycline present in the matrix. Antibiotic loaded PLA membrane (S6) presented a burst release of 3% and a sustained release until 180 min, where it reached equilibrium with a cumulative release of 22%, while the gelatin membrane added with aloe vera and the antibiotic (S4) presented an initial release of 12% of the antibiotic, followed by a sustained discharge until 150 min, where a release of 58% of the antibiotic contained in the matrix was reached. The coaxial membrane shows an initial release of 5%, followed by a sustained release until reaching equilibrium of 47.5% after 140 min. Comparing the release of tetracycline from S3 and S4, similar values of release percentage and equilibrium time can be noted, confirming that the presence of aloe vera in the fibers does not affect the discharge of tetracycline into the medium.

The release of aloe vera mucilage from the prepared systems is shown in Figure 6B, and in the case of the membrane prepared using simple configuration (S2), an initial release of 58% of the mucilage is seen, followed by a constant release until equilibrium, reached after 100 min, where 80% of the active agents present in the membrane were released, while in the coaxial system (C3), 32% is initially released followed by a constant release until equilibrium is reached in 100 min, managing to accumulate the output of 70% of the active agent.

The adjustment of the kinetics to reported release models (zero order, Higuchi, and Peppas) is summarized in Table 2. In the case of tetracycline release, the S3 membrane adjusts with a higher correlation coefficient to the model proposed by Higuchi, so the discharge from this system is presumed to be due to diffusion of the antibiotic from the membrane to the release medium, while the S4 membrane, its best fit is in the model proposed by Korsmeyer−Peppas; however, the diffusion coefficient n = 0.5952 is close to the value n = 0.5, which suggests that the output can be explained by the diffusion of the active agent toward the release medium with a small contribution from the erosion/dissolution factor of the matrix, and in the case of the coaxial membrane C3, a coefficient of n = 0.471 is observed, which, like S4, suggests diffusion, however, comparing the values of n and k for these systems, values are lower for C3, which implies a lower release speed, in concordance with our previous work.[63]

In the case of aloe vera mucilage, in the membrane prepared in a simple configuration, a better fit to the model proposed by

https://doi.org/10.1021/acsomega.4c01016
ACS Omega 2024, 9, 41157−41170

(A)

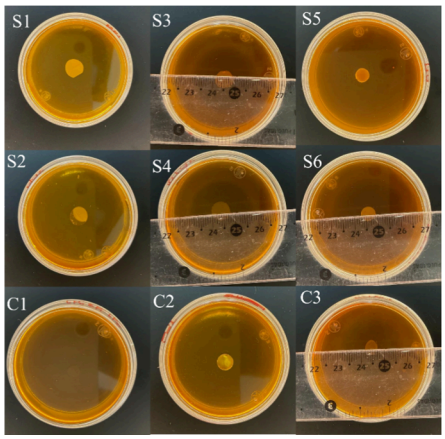

(B)

System	Inhibition zone ±σ (mm)
S1	-
S2	-
S3	26.1 ± 1.10
S4	28.1 ± 0.67
S5	-
S6	25.2 ± 1.30
C1	-
C2	-
C3	23.8 ± 0.99

Figure 7. Antimicrobial activity of electrospun membranes prepared on a single configuration (S1−S6) and coaxial configuration (C1−C3). (A) Agar diffusion test of polymeric membranes against *S. aureus* at 24 h of incubation. (B) Inhibition halo ± σ (mm).

Higuchi is found, which suggests a release by diffusion, while in the coaxial membrane, similar correlation coefficients are found between the models, and the best fit is found with the zero order model, which suggests a release due to erosion or dissolution of the matrix; in this case, the shell of the fibers is composed of PLA, which can be hydrolyzed and thus explains the mechanism by which the active agent is discharged into the release medium. Comparing the release of antibiotic from single and coaxial systems, the burst release and the antibiotic release rate are lower in the coaxial system, which makes it a suitable material for controlled release applications.

Antimicrobial Activity. Figure 7 shows the results of the antimicrobial activity test of the single and coaxial scaffolds against *S. aureus*. The antibiotic-free membranes do not show activity against the bacteria, while those enriched with the drug present inhibition zones of bacteria growth, which shows that the treatment that the membranes received, such as electrospinning and the subsequent cross-linking reaction, did not affect their activity. When the antimicrobial activity of S3 and S4 membranes was compared, S3 membranes showed an inhibition zone of 26.1 mm, while S4 membranes showed a halo of 28.1 mm.

This finding indicates that S4 membranes exhibit greater antimicrobial activity, which can be attributed to the effects of the drug itself and the additional components present in the mucilage. Components from the aloe vera mucilage as polysaccharides and phenolic compounds can enhance the antimicrobial effect of the tetracycline itself as reported by Sartini et al.,[64] who explained the interaction between natural components and the conventional antibiotic. It has been reported that flavones contained in natural products such as aloe vera has enhanced the effect of tetracycline, because of the interaction of hydroxyl groups with the antibiotic structure,[65] demonstrating the synergistic effect of the drug and the natural compounds. Comparing S4 and C3 membranes, the coaxial configuration leads to lower activity due to slower diffusion in the media, as observed in drug delivery studies.

Cell Culture. In tissue engineering applications, it is important to evaluate materials at culture times suitable for the application. Mammalian adipose-derived stem cells (ASCs) were cultured in contact with polymeric scaffolds. To assess the cytotoxicity of the scaffolds, cell viability was measured using the Presto Blue test, and the results are shown in Figure 8A. In general, the viability increased slightly as the days passed, this due to the adaptation of the cells. For all cases, viability greater than 90% was obtained, which qualifies these materials as nontoxic to these cells, and slightly greater on the aloe vera-loaded fibers. One of the cellular components of the skin is fibroblasts, which are part of the connective tissue such as tendons as well as the skin itself. The evaluation of candidate materials to be used as

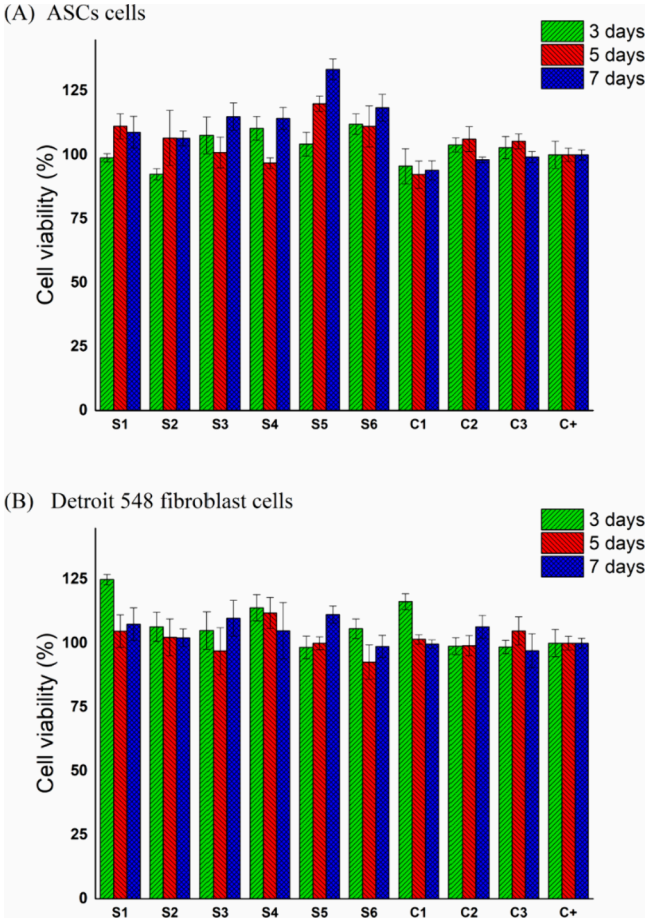

Figure 8. Cell viability of cells cultured at 3, 5, and 7 days of incubation in contact with polymeric scaffolds prepared on single configuration (S1−S4) and coaxial configuration (C1−C3). (A) Viability of mammalian adipose stem cells (ASCs) and (B) viability of the Detroit 548 Human Skin fibroblast.

https://doi.org/10.1021/acsomega.4c01016
ACS Omega 2024, 9, 41157−41170

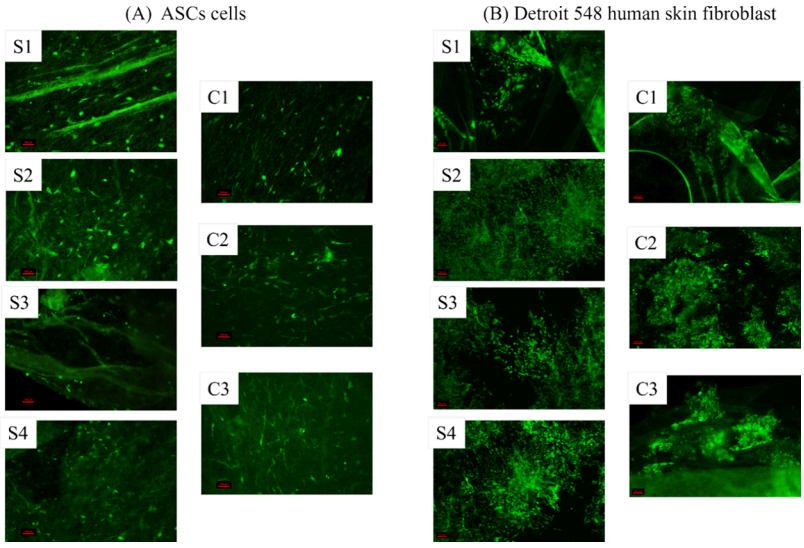

Figure 9. Overlay images from live−dead assay of cultured scaffolds prepared on single configuration (S1−S4) and coaxial configuration (C1−C3) at day 7. (A) ASCs cell culture and (B) Detroit 548 cells culture. Images were taken at 10×. Scale bar is 100 μm.

dressings or scaffolds in tissue engineering must be evaluated in cell line models like those that would be in contact in the in vivo application. The evaluation of membranes based on gelatin, PLA, aloe vera, and tetracycline in contact with Detroit 548 human skin fibroblasts is shown in Figure 8B. For all cases, viabilities greater than 90% were obtained, with greater values of viability on aloe vera-loaded membranes. Both the membranes and their components are considered safe materials to be in contact with applications where these types of cells are found, such as human skin.

Live−Dead Assay. Important aspects in the evaluation of materials in tissue engineering are the viability and cell adhesion. The calcein-ethidium bromide staining technique was used to visualize the cells adhered on the polymeric membranes, and the results of this test on day 7 of culture in adipose stem cells (ASCs) and Detroit 548 fibroblasts are found in Figure 9. The figure shows the overlay image obtained by the fluorescence of calcein and ethidium bromide on cultured gelatin-based membranes, where the green fluorescence shows viable cells and red is nonviable due to fluorescence of ethidium bromide from interaction with DNA from damaged cells. Pure PLA membranes were not suitable for cell staining since autofluorescence of the material was higher than cell staining fluorescence on these scaffolds.

Figure 9A shows the culture of ASCs cells; for this, in the case of gelatin fibers, good adhesion and viability can be seen, since abundant cells are observed with no cells on the red channel, while for the fibers added with aloe vera, more cells are observed. In the gelatin scaffolds enriched with tetracycline, less cells can be observed with fluorescence in the green color, which may be explained considering adaptation to the cells on the media. On the membrane that contains the aloe vera, in addition to the drug, the number of cells is higher in comparison with only antibiotic-loaded fibers, so it is presumed that the biocompatible effect of aloe vera is higher than the effect of the antibiotic, and this effect can be observed in both types of fibers, single, and coaxial. Figure 9B shows the culture of Detroit 548 cells. In all cases, it is possible to notice good viability due to the absence of fluorescence in the red channel; however, the confluence of the cells is different depending on the type of scaffold. For the gelatin and coaxial scaffold, good confluence on the live channel and no red cells are observed, which indicates cell growth and division; for the aloe vera-enriched scaffolds, a greater confluence and stacking of cells are observed, which implies the synthesis of extracellular membrane, and it is an indication of a suitable scaffold for tissue growth. The addition of the antibiotic has a negative effect on the cells, as can be seen on the S3 membrane, which shows lower confluence; however, when both the natural agent and the drug are added, as in S4 and C3 membranes, the effect on the cells is favorable. On aloe vera, antibiotic loaded fibers greater confluence than the unloaded scaffold can be seen, so the negative effect of the antibiotic can be diminished using the natural agent and be suitable for applications where it is necessary to include antibiotic in the formulation.

Cell Proliferation. The images in Figures 10 and11 show the sequence of phalloidin-Hoechst staining, carried out on the

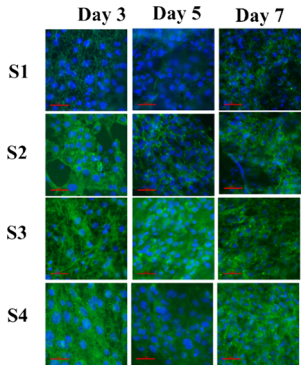

Figure 10. Cell staining of nucleus (blue) and actin filaments (green) of cultured cells on single electrospun membranes (S1−S4) at days 3, 5, and 7 of culture. Images were taken at 20×. Scale bar is 50 μm.

culture of Detroit 548 human skin fibroblast on gelatin-based scaffolds prepared using single and coaxial configuration after 3, 5, and 7 days of culture. The actin filaments are colored in the green channel, while the cell nuclei from the cells are shown in blue. For the culture of Detroit 548 human skin fibroblasts, adhered cells with good confluence were found in all cases;

https://doi.org/10.1021/acsomega.4c01016
ACS Omega 2024, 9, 41157−41170

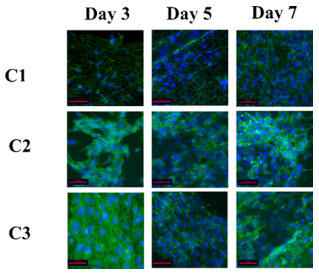

Figure 11. Cell staining of nucleus (blue) and actin filaments (green) of cultured cells on coaxial electrospun membranes (C1−C3) at days 3, 5, and 7 of culture. Images taken at 20×. Scale bar is 50 μm.

however, the morphology and levels of confluence, although high for all cases, were different.

The culture of cells above scaffolds prepared on a single configuration is presented in Figure 10. S1 and S3 scaffolds presented results with elongated cells and good confluence of fibroblasts, which makes them candidate materials for tissue engineering applications, while the S2 and S4 scaffolds showed greater compatibility with cells, due to their confluence, increased cell density, and better cell organization, which has been reported to occur when cells are grown at high confluence, making these materials suitable for dermal tissue regeneration applications.

In the case of coaxial membranes (Figure 11) for all cases, it was possible to observe cells adhered to the scaffolds; however, the morphology and confluence were different. In the C1 scaffold, elongated cells are observed from day 3 of culture, and the increase in confluence is shown at days 5 and 7. For aloe vera-enriched membranes (C2), elongated and confluent cells are observed on the scaffolds since day 3, attributed to the biocompatibility of the aloe vera on the membranes. In tetracycline and aloe vera enriched fibers (C3), elongated and confluent cells are observed since day 3 also, which is attributed to the biocompatibility effect of the aloe vera above the antibiotic. C2 and C3 showed more confluence of cells than C1; this behavior is attributed to the morphology of the porous membranes, which mimics the extracellular matrix, as shown in Figure 3.

3D reconstruction of stained scaffolds from human skin fibroblast cultures at day 7 is shown in Figure 12, and cell distribution and actin filament saturation can be noted. Gelatin single scaffold S1 and coaxial scaffold C1 show homogeneous distribution of cells due to nuclei blue staining and low values of actin, which increases when aloe vera is added to the membranes and decreases with the addition of the antibiotic on the S2 and S3 scaffolds, respectively. When both compounds are added to the membranes the distribution of cells and the actin filaments is equilibrated, the suppressor effect of antibiotic is attenuated by the aloe vera mucilage. In coaxial prepared fibers, proliferation is augmented when aloe vera is added to the preparations as seen in C2 and this effect is not attenuated with the incorporation of antibiotic for the C3 membranes.

CONCLUSIONS

Electrospun gelatin and PLA-based scaffolds were prepared on single and coaxial configurations. Fiber mats were enriched with aloe vera mucilage, locally obtained from leaves collected in Hermosillo, Sonora, and hydrochloride tetracycline. Addition of active compounds to the fibers modified the diameter of the

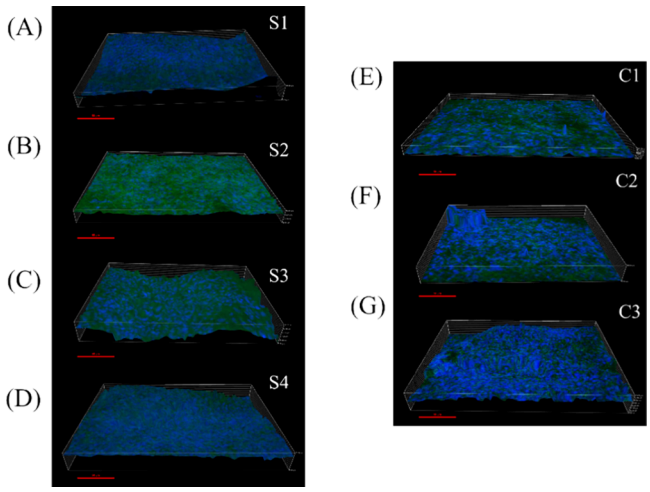

Figure 12. 3D reconstruction of stained Detroit 548 fibroblast cultured scaffolds at day 7 on (A) gelatin S1, (B) gelatin-aloe vera S2, (C) gelatin-tetracycline S3, (D) gelatin-aloe vera-tetracycline S4, (E) coaxial C1, (F) coaxial- aloe vera C2, and (G) coaxial aloe vera-tetracycline C3. Images were taken at 20×. Scale bar is 10 μm.

fibers due to interactions between gelatin and the incorporated compounds.

Cross-linking reaction, performed by the glutaraldehyde-saturated vapor method, modified the physicochemical characteristics of the obtained membranes. Morphology of the fibers changed from the cylinder structure to ribbon morphology, and porous structures were also observed, attributed to the interaction between gelatin amine groups across the chains. Additional evidence of the interaction was wavenumber shifts on the carbonyl group and the increase of the thermal stability of the membranes. It was found that drug release can be adjusted using a coaxial configuration, showing a controlled release of the antibiotic in comparison with the single fibers.

Biological assay results showed that gelatin-based membranes have potential for use in various tissue engineering applications such as drug delivery, wound healing, and tissue formation with focus on burn recovery and diabetic foot treatments. The compatibility with mammalian adipose stem cells was first evidenced in which it was discovered that the most suitable membranes for cell culture applications resulted in those that were composed of gelatin in a simple configuration and added with aloe vera and tetracycline. On Detroit 548 human skin fibroblast cultures, it was found that aloe vera improved actin production and therefore the generation of tissue by the cells, while the antibiotic slowed growth; however, a dressing that contains both substances has a high potential to be used in special applications such as burns and diabetic foot. Scaffolds containing tetracycline showed antimicrobial activity against *S. aureus*, being higher in those containing both the natural compound and the drug. The use of natural active agents promotes compatibility in polymeric scaffolds, while the use of conventional drugs guarantees antibiotic action, so it is recommended to include both compounds in the material.

We investigated the production and performance of single- and coaxial electrospun fibers. Both types of systems showed good properties and performance during physicochemical and biological evaluations. Nevertheless, coaxial systems presented a more sustained release of active compounds, so the coaxial loaded system C3 is recommended for applications where the

https://doi.org/10.1021/acsomega.4c01016
ACS Omega 2024, 9, 41157−41170

drug delivery is important, and even multiple-drug systems could be prepared. The loaded single system S4 is recommended for wound dressing applications where the antimicrobial properties are needed as the antibiotic is rapidly discharged and the bioactivity of aloe vera is maintained for tissue regeneration and wound recovery.

AUTHOR INFORMATION

Corresponding Author

María Mónica Castillo Ortega − *Departamento de Investigación en Polímeros y Materiales, Universidad de Sonora, Hermosillo, Sonora 83000, México;* orcid.org/0000-0003-3522-1105; Email: monica.castillo@unison.mx

Authors

Damian Francisco Plascencia Martinez − *Departamento de Investigación en Polímeros y Materiales, Universidad de Sonora, Hermosillo, Sonora 83000, México*

Jesús Manuel Quiroz Castillo − *Departamento de Investigación en Polímeros y Materiales, Universidad de Sonora, Hermosillo, Sonora 83000, México;* orcid.org/0000-0002-8810-6162

Alida Ospina Orejarena − *Centro de Tecnología de Sigma Alimentos, Apodaca, NL 66629, México*

Alfonso Pérez Gallardo − *Centro de Tecnología de Sigma Alimentos, Apodaca, NL 66629, México*

Emilio Méndez Merino − *Centro de Tecnología de Sigma Alimentos, Apodaca, NL 66629, México*

Gerardo Asael Trimmer López − *Facultad de Ingeniería Mecánica y Eléctrica, Universidad Autónoma de Nuevo León, San Nicolás de los Garza 66455, México*

Itzel Yanira López Peña − *Centro de Investigación en Alimentación y Desarrollo, Hermosillo, Sonora 83304, México*

Diego Hernández Martínez − *Departamento de Investigación en Polímeros y Materiales, Universidad de Sonora, Hermosillo, Sonora 83000, México*

Karla Alejandra López Gastelum − *Centro de Investigación en Alimentación y Desarrollo, Hermosillo, Sonora 83304, México;* orcid.org/0000-0001-5029-7330

Abraham Alejandro Leyva Verduzco − *Departamento de Investigación en Polímeros y Materiales, Universidad de Sonora, Hermosillo, Sonora 83000, México*

Antonio S. Ledezma − *Materiales Avanzados, Centro de Investigación en Química Aplicada, Saltillo, Coahuila 25294, México*

Complete contact information is available at: https://pubs.acs.org/10.1021/acsomega.4c01016

Author Contributions

D.F.P.M. M.M.C.O, I.Y.L.P., A.A.L.V., and A.O.O. were responsible for conceptualization; A.S.L. P. J.M.Q.C., K.A.L.G., G.A.T.L., M.M.C.O., and D.H.M. were responsible for methodology; M.M.C.O., E.M.M., and A.P.G. were responsible for resources; D.F.P.M., J.M.Q.C., I.Y.L.P, M.M.C.O., and A.O.O. were responsible for writing the original draft preparation; A.P.G., A.S.L.P., D.H.M., K.A.L.G., G.A.T.L., A.A.L.V., D.F.P.M., J.M.Q.C., and M.M.C.O. were responsible for writing the review and editing; A.S.L.P., M.M.C.O., A.A.L.V., A.P.G., and E.M.M were responsible for supervision. The manuscript was written through contributions of all authors. All authors have given approval to the final version of the manuscript.

Notes

The authors declare no competing financial interest.

ACKNOWLEDGMENTS

Damian Francisco Plascencia Martínez acknowledges CONAHCYT (Consejo Nacional de Humanidades, Ciencia y Tecnología, México) for the financial support provided for his graduate studies during this study and Sigma Alimentos for the support and laboratory facilities for the experiments during the doctoral research stay. Authors thank Jesus Angel Cepeda from Centro de Investigación en Química Aplicada (CIQA, Saltillo) for the technical support on the morphological characterization of coaxial fibers and Irela Santos Sauceda from Universidad de Sonora for the support in the thermal characterization.

REFERENCES

(1) Deutsch, C.; Edwards, D.; Myers, S. Wound Dressings. *Br J. Hosp Med.* **2017**, *78* (7), C103−C109.

(2) Obagi, Z.; Damiani, G.; Grada, A.; Falanga, V. Principles of Wound Dressings: A Review. *Surg. Technol. Int.* **2019**, *35*, 50−57.

(3) Griffith, L. G.; Naughton, G. Tissue Engineering−Current Challenges and Expanding Opportunities. *Science (1979)* **2002**, *295* (5557), 1009−1014.

(4) Roseti, L.; Parisi, V.; Petretta, M.; Cavallo, C.; Desando, G.; Bartolotti, I.; Grigolo, B. Scaffolds for Bone Tissue Engineering: State of the Art and New Perspectives. *Materials Science and Engineering C* **2017**, *78*, 1246−1262. Elsevier Ltd. September 1

(5) Stratton, S.; Shelke, N. B.; Hoshino, K.; Rudraiah, S.; Kumbar, S. G. Bioactive Polymeric Scaffolds for Tissue Engineering. *Bioact Mater.* **2016**, *1* (2), 93−108.

(6) Biswal, T. Biopolymers for Tissue Engineering Applications: A Review. *Mater. Today: Proc.* **2019**, *41*, 397−402. Elsevier Ltd.

(7) Volpi, M.; Paradiso, A.; Costantini, M.; Święszkowski, W. Hydrogel-Based Fiber Biofabrication Techniques for Skeletal Muscle Tissue Engineering. *ACS Biomaterials Science and Engineering* **2022**, *8*, 379−405. American Chemical Society February 14

(8) Rodrigues, M.; Kosaric, N.; Bonham, C. A.; Gurtner, G. C. Wound Healing: A Cellular Perspective. *Physiol Rev.* **2019**, *99* (1), 665−706.

(9) Liu, X.; Xu, H.; Zhang, M.; Yu, D. G. Electrospun Medicated Nanofibers for Wound Healing: Review. *Membranes (Basel)* **2021**, *11* (10). 770.

(10) Xiao, H.; Chen, X.; Liu, X.; Wen, G.; Yu, Y. Recent Advances in Decellularized Biomaterials for Wound Healing. *Mater. Today Bio* **2023**, *19*, No. 100589.

(11) Thorvaldsson, A.; Stenhamre, H.; Gatenholm, P.; Walkenström, P. Electrospinning of Highly Porous Scaffolds for Cartilage Regeneration. *Biomacromolecules* **2008**, *9* (3), 1044−1049.

(12) Gizaw, M.; Thompson, J.; Faglie, A.; Lee, S.-Y.; Neuenschwander, P.; Chou, S.-F. Electrospun Fibers as a Dressing Material for Drug and Biological Agent Delivery in Wound Healing Applications. *Bioengineering* **2018**, *5* (1), 9.

(13) Abrigo, M.; McArthur, S. L.; Kingshott, P. Electrospun Nanofibers as Dressings for Chronic Wound Care: Advances, Challenges, and Future Prospects. *Macromol. Biosci* **2014**, *14* (6), 772−792.

(14) Raina, N.; Pahwa, R.; Khosla, J. K.; Gupta, P. N.; Gupta, M. Polycaprolactone-Based Materials in Wound Healing Applications. *Polym. Bull.* **2022**, *1*, 7041−7063. Springer Science and Business Media Deutschland GmbH September

(15) Barbosa, R.; Villarreal, A.; Rodriguez, C.; De Leon, H.; Gilkerson, R.; Lozano, K. Aloe Vera Extract-Based Composite Nanofibers for Wound Dressing Applications. *Materials Science and Engineering C* **2021**, *124* (March), No. 112061.

(16) Shahravi, Z.; Mehdikhani, M.; Amirkhani, M. A.; Mollapour Sisakht, M.; Farsaei, S. Multifunctional Electrospun Polyvinyl Alcohol/Gellan Gum/Polycaprolactone Nanofibrous Membrane Containing

https://doi.org/10.1021/acsomega.4c01016
ACS Omega 2024, 9, 41157−41170

Pentoxifylline to Accelerate Wound Healing. *Polym. Bull.* **2023**, *80* (2), 2217−2237.
(17) Kanakubo, Y.; Watanabe, C.; Yamamoto, J.; Yanagisawa, N.; Sakuta, H.; Nikoubashman, A.; Yanagisawa, M. Cell-Sized Confinements Alter Molecular Diffusion in Concentrated Polymer Solutions Due to Length-Dependent Wetting of Polymers. *ACS Materials Au* **2023**. 3442.
(18) Palomares, D.; Ammann, K. R.; Saldana Perez, J. J.; Gomez, A.; Barreda, A.; Russell-Cheung, A.; Martin, A.; Tran, P. L.; Hossainy, S.; Slepian, R. C.; Hossainy, S. F. A.; Slepian, M. J. Patterned Electrospinning: A Method of Generating Defined Fibrous Constructs Influencing Cell Adhesion and Retention. *ACS Appl. Bio Mater.* **2021**, *4* (5), 4084−4093.
(19) He, C.; Yu, B.; Lv, Y.; Huang, Y.; Guo, J.; Li, L.; Chen, M.; Zheng, Y.; Liu, M.; Guo, S.; Shi, X.; Yang, J. Biomimetic Asymmetric Composite Dressing by Electrospinning with Aligned Nanofibrous and Micropatterned Structures for Severe Burn Wound Healing. *ACS Appl. Mater. Interfaces* **2022**, *14* (29), 32799−32812.
(20) Mulholland, E. J. Electrospun Biomaterials in the Treatment and Prevention of Scars in Skin Wound Healing. *Front. Bioeng. Biotechnol.* **2020**, *8*, 481.
(21) Rosales-Ibáñez, R.; Viera-Ruiz, A. E.; Cauich-Rodríguez, J. V.; Carrillo-Escalante, H. J.; González-González, A.; Rodríguez-Martínez, J. J.; Hernández-Sánchez, F. Electrospun/3D-Printed PCL Bioactive Scaffold for Bone Regeneration. *Polym. Bull.* **2023**, *80* (3), 2533−2552.
(22) Chen, S.; Li, R.; Li, X.; Xie, J. Electrospinning: An Enabling Nanotechnology Platform for Drug Delivery and Regenerative Medicine. *Adv. Drug Deliv Rev.* **2018**, *132*, 188−213.
(23) Duan, M.; Sun, J.; Huang, Y.; Jiang, H.; Hu, Y.; Pang, J.; Wu, C. Electrospun Gelatin/Chitosan Nanofibers Containing Curcumin for Multifunctional Food Packaging. *Food Science and Human Wellness* **2023**, *12* (2), 614−621.
(24) Chen, H.; Su, J.; Brennan, C. S.; Van der Meeren, P.; Zhang, N.; Tong, Y.; Wang, P. Recent Developments of Electrospun Zein Nanofibres: Strategies, Fabrication and Therapeutic Applications. *Mater. Today Adv.* **2022**, *16*, No. 100307.
(25) Shokrani, H.; Shokrani, A.; Jouyandeh, M.; Seidi, F.; Gholami, F.; Kar, S.; Munir, M. T.; Kowalkowska-Zedler, D.; Zarrintaj, P.; Rabiee, N.; Saeb, M. R. Green Polymer Nanocomposites for Skin Tissue Engineering. *ACS Appl. Bio Mater.* **2022**, *5* (5), 2107−2121.
(26) Wang, Y.; Wang, Z.; Dong, Y. Collagen-Based Biomaterials for Tissue Engineering. *ACS Biomater Sci. Eng.* **2023**, *9* (3), 1132−1150.
(27) Elsadek, N. E.; Nagah, A.; Ibrahim, T. M.; Chopra, H.; Ghonaim, G. A.; Emam, S. E.; Cavalu, S.; Attia, M. S. Electrospun Nanofibers Revisited: An Update on the Emerging Applications in Nanomedicine. *Materials* **2022**, *15* (5), 1934.
(28) Mitxelena-Iribarren, O.; Riera-Pons, M.; Pereira, S.; Calero-Castro, F. J.; Castillo Tuñón, J. M.; Padillo-Ruiz, J.; Mujika, M.; Arana, S. Drug-Loaded PCL Electrospun Nanofibers as Anti-Pancreatic Cancer Drug Delivery Systems. *Polym. Bull.* **2023**. *807*763.
(29) Kaniuk, Ł.; Berniak, K.; Lichawska-Cieślar, A.; Jura, J.; Karbowniczek, J. E.; Stachewicz, U. Accelerated Wound Closure Rate by Hyaluronic Acid Release from Coated PHBV Electrospun Fiber Scaffolds. *J. Drug Delivery Sci. Technol.* **2022**, *77*, No. 103855.
(30) Greenfeld, I.; Zussman, E. Controlling the Nanostructure of Electrospun Polymeric Fibers. In *Electrospinning for High Performance Sensors*; Macagnano, A.; Zampetti, E.; Kny, E., Eds.; Springer International Publishing: Cham, 2015; pp 35−64 DOI: 10.1007/978-3-319-14406-1_2.
(31) Zafar, M.; Najeeb, S.; Khurshid, Z.; Vazirzadeh, M.; Zohaib, S.; Najeeb, B.; Sefat, F. Potential of Electrospun Nanofibers for Biomedical and Dental Applications. *Materials* **2016**, *9* (2), 73.
(32) Altinkok, C.; Sagdic, G.; Daglar, O.; Ercan Ayra, M.; Yuksel Durmaz, Y.; Durmaz, H.; Acik, G. A New Strategy for Direct Solution Electrospinning of Phosphorylated Poly(Vinyl Chloride)/Polyethyleneimine Blend in Alcohol Media. *Eur. Polym. J.* **2023**, *183*.
(33) Sohrabi, M.; Abbasi, M.; Ansar, M. M.; Soltani Tehrani, B. Evaluation of Electrospun Nanofibers Fabricated Using PCL/PVP and PVA/β-TCP as Potential Scaffolds for Bone Tissue Engineering. *Polym. Bull.* **2022**, *79* (10), 8397−8413.
(34) Zakrzewska, A.; Zargarian, S. S.; Rinoldi, C.; Gradys, A.; Jarząbek, D.; Zanoni, M.; Gualandi, C.; Lanzi, M.; Pierini, F. Electrospun Poly(Vinyl Alcohol)-Based Conductive Semi-Interpenetrating Polymer Network Fibrous Hydrogel: A Toolbox for Optimal Cross-Linking. *ACS Materials Au* **2023**. 3464.
(35) Alharbi, H. F.; Luqman, M.; Khalil, K. A.; Elnakady, Y. A.; Abd-Elkader, O. H.; Rady, A. M.; Alharthi, N. H.; Karim, M. R. Fabrication of Core-Shell Structured Nanofibers of Poly (Lactic Acid) and Poly (Vinyl Alcohol) by Coaxial Electrospinning for Tissue Engineering. *Eur. Polym. J.* **2018**, *98*, 483−491.
(36) Baghali, M.; Ziyadi, H.; Faridi-Majidi, R. Fabrication and Characterization of Core−Shell TiO2-Containing Nanofibers of PCL-Zein by Coaxial Electrospinning Method as an Erythromycin Drug Carrier. *Polym. Bull.* **2022**, *79* (3), 1729−1749.
(37) Gün Gök, Z. Synthesis and Characterization of Polyvinyl Alcohol−Silk Sericin Nanofibers Containing Gelatin-Capped Silver Nanoparticles for Antibacterial Applications. *Polym. Bull.* **2022**, *79* (11), 10357−10376.
(38) Etxabide, A.; Akbarinejad, A.; Chan, E. W. C.; Guerrero, P.; de la Caba, K.; Travas-Sejdic, J.; Kilmartin, P. A. Effect of Gelatin Concentration, Ribose and Glycerol Additions on the Electrospinning Process and Physicochemical Properties of Gelatin Nanofibers. *Eur. Polym. J.* **2022**, *180*, No. 111597.
(39) Jirkovec, R.; Kalous, T.; Brayer, W. A.; Stanishevky, A. V.; Chvojka, J. Production of Gelatin Nanofibrous Layers via Alternating Current Electrospinning. *Mater. Lett.* **2019**, *252*, 186−190.
(40) Campa-Siqueiros, P. I.; Madera-Santana, T. J.; Ayala-Zavala, J. F.; López-Cervantes, J.; Castillo-Ortega, M. M.; Herrera-Franco, P. J.; Quintana-Owen, P. Co-Electrospun Nanofibers of Gelatin and Chitosan−Polyvinyl Alcohol−Eugenol for Wound Dressing Applications. *Polym. Bull.* **2023**. *803*611.
(41) Popelka, A.; Abdulkareem, A.; Mahmoud, A. A.; Nassr, M. G.; Al-Ruweidi, M. K. A. A.; Mohamoud, K. J.; Hussein, M. K.; Lehocky, M.; Vesela, D.; Humpolíček, P.; Kasak, P. Antimicrobial Modification of PLA Scaffolds with Ascorbic and Fumaric Acids via Plasma Treatment. *Surf. Coat. Technol.* **2020**, *400* (May), No. 126216.
(42) Zhang, B.; Wang, L.; Song, P.; Pei, X.; Sun, H.; Wu, L.; Zhou, C.; Wang, K.; Fan, Y.; Zhang, X. 3D Printed Bone Tissue Regenerative PLA/HA Scaffolds with Comprehensive Performance Optimizations. *Mater. Des* **2021**, *201*, No. 109490.
(43) Suner, S. C.; Oral, A.; Yildirim, Y. Design of Poly(Lactic) Acid/Gelatin Core-Shell Bicomponent Systems as a Potential Wound Dressing Material. *J. Mech Behav Biomed Mater.* **2024**, *150*, No. 106255.
(44) Chen, H.; Zhang, H.; Shen, Y.; Dai, X.; Wang, X.; Deng, K.; Long, X.; Liu, L.; Zhang, X.; Li, Y.; Xu, T. Instant In-Situ Tissue Repair by Biodegradable PLA/Gelatin Nanofibrous Membrane Using a 3D Printed Handheld Electrospinning Device. *Front. Bioeng. Biotechnol.* **2021**, *9*, No. 684105.
(45) WANG, H.; WANG, L.; FAN, K.; PAN, G. Tetracycline Natural Products: Discovery, Biosynthesis and Engineering. *Chin J. Nat. Med.* **2022**, *20* (10), 773−794.
(46) Ranjbar-Mohammadi, M.; Zamani, M.; Prabhakaran, M. P.; Bahrami, S. H.; Ramakrishna, S. Electrospinning of PLGA/Gum Tragacanth Nanofibers Containing Tetracycline Hydrochloride for Periodontal Regeneration. *Materials Science and Engineering C* **2016**, *58*, 521−531.
(47) Hashemi, H.; Rahimzadeh, G.; Saeedi, M.; Ghadami, F.; Rafati, A.; Gill, P. Ultra-Structural Characteristics of Aloe Vera-Based Nanofibers as Mrsa-Phage Nanocarriers. *Biointerface Res. Appl. Chem.* **2022**, *12* (2), 2152−2161.
(48) Liu, Y.; Fan, J.; Lv, M.; She, K.; Sun, J.; Lu, Q.; Han, C.; Ding, S.; Zhao, S.; Wang, G.; Zhang, Y.; Zang, G. Photocrosslinking Silver Nanoparticles−Aloe Vera−SilkFibroin Composite Hydrogel for Treatment of Full-Thickness Cutaneous Wounds. *Regener. Biomater.* **2021**, *8* (6), rbab048.

https://doi.org/10.1021/acsomega.4c01016
ACS Omega 2024, 9, 41157−41170

(49) Sánchez-Machado, D. I.; López-Cervantes, J.; Sendón, R.; Sanches-Silva, A. Aloe Vera: Ancient Knowledge with New Frontiers. *Trends Food Sci. Technol.* **2017**, *61*, 94−102.
(50) Maan, A. A.; Nazir, A.; Khan, M. K. I.; Ahmad, T.; Zia, R.; Murid, M.; Abrar, M. The Therapeutic Properties and Applications of Aloe Vera: A Review. *J. Herb. Med.* **2018**, *12*, 1−10.
(51) Zarandona, I.; Minh, N. C.; Trung, T. S.; de la Caba, K.; Guerrero, P. Evaluation of Bioactive Release Kinetics from Crosslinked Chitosan Films with Aloe Vera. *Int. J. Biol. Macromol.* **2021**, *182*, 1331−1338.
(52) Medina-Torres, L.; Calderas, F.; Minjares, R.; Femenia, A.; Sánchez-Olivares, G.; Gónzalez-Laredo, F. R.; Santiago-Adame, R.; Ramirez-Nuñez, D. M.; Rodríguez-Ramírez, J.; Manero, O. Structure Preservation of Aloe Vera (Barbadensis Miller) Mucilage in a Spray Drying Process. *LWT - Food Science and Technology* **2016**, *66*, 93−100.
(53) Ngamsurach, P.; Praipipat, P. Antibacterial Activities against Staphylococcus Aureus and Escherichia Coli of Extracted Piper Betle Leaf Materials by Disc Diffusion Assay and Batch Experiments. *RSC Adv.* **2022**, *12* (40), 26435−26454.
(54) Vásquez-López, C.; Castillo-Ortega, M. M.; Chan-Chan, L. H.; Lagarda-Díaz, I.; Giraldo-Betancur, A. L.; Rodríguez-Félix, D. E.; Encinas-Encinas, J. C.; Martínez-Barbosa, M. E.; Cadenas-Pliego, G.; Cauich-Rodríguez, J. V.; Herrera-Franco, P. J. Polyurethane Electrospun Membranes with Hydroxyapatite-Vancomycin for Potential Application in Bone Tissue Engineering and Drug Delivery. *J. Appl. Polym. Sci.* **2022**, *139* (14), 51893.
(55) Journal, A.; Sciences, B.; Publications, S Ramachandr, C. T.; Rao, P. S. Processing of Aloe Vera Leaf Gel: A Review. *Am. J. Agric Biol. Sci.* **2008**, *3* (2), 502−510. Department of Agricultural and Food Engineering, Indian Institute of Technology, Kharagpur-721302, India
(56) Baghersad, S.; Hajir Bahrami, S.; Mohammadi, M. R.; Mojtahedi, M. R. M.; Milan, P. B. Development of Biodegradable Electrospun Gelatin/Aloe-Vera/Poly(E-caprolactone) Hybrid Nanofibrous Scaffold for Application as Skin Substitutes. *Materials Science and Engineering C* **2018**, *93*, 367−379.
(57) Abbasi, M. S. A.; Tahir, M. A.; Meer, S. FTIR Spectroscopic Study of Aloe Vera Barbadensis Mill Buds. *Asian Journal of Chemical Sciences* **2020**, 1−6.
(58) Mohd Nizam, N. H.; Mohammad Rawi, N. F.; Mhd Ramle, S. F.; Abd Aziz, A.; Abdullah, C. K.; Rashedi, A.; Mohamad Kassim, M. H. Physical, Thermal, Mechanical, Antimicrobial and Physicochemical Properties of Starch Based Film Containing Aloe Vera: A Review. *Journal of Materials Research and Technology* **2021**, *15*, 1572−1589.
(59) Simal, S.; Rossello, C.; Femenia, A.; Sánchez, E. Compositional Features of Polysaccharides from Aloe Vera (Aloe Barbadensis Miller) Plant Tissues. *Carbohydr. Polym.* **1999**, *39*, 109−117.
(60) Imani, R.; Rafienia, M.; Hojjati Emami, S. Synthesis and Characterization of Glutaraldehyde-Based Crosslinked Gelatin as a Local Hemostat Sponge in Surgery: An in Vitro Study. *Bio-Med. Mater. Eng.* **2013**, *23* (3), 211−224.
(61) Chen, G.; Ushida, T.; Tateishi, T. Scaffold Design for Tissue Engineering. *Macromol. Biosci.* **2002**, *2*, 67.
(62) Stratton, S.; Shelke, N. B.; Hoshino, K.; Rudraiah, S.; Kumbar, S. G. Bioactive Polymeric Scaffolds for Tissue Engineering. *Bioactive Materials.* **2016**, *1*, 93−108. KeAi Communications Co. December 1
(63) López-Peña, I. Y.; Castillo-Ortega, M. M.; Plascencia-Martínez, D. F.; Félix-Núñez, A.; Rodríguez-Félix, D. E.; Del Castillo-Castro, T.; Encinas-Encinas, J. C.; Santacruz-Ortega, H.; Rodríguez-Félix, F.; Cauich-Rodríguez, J. V.; Burruel-Ibarra, S.; Hernandez-Martínez, D.; Quiroz-Castillo, J. M. Study of the Release Kinetics of (−) Epicatechin: Effect of Its Location within the Fiber or Sphere. *J. Appl. Polym. Sci.* **2019**, *136* (10), 47166.
(64) Sartini, S.; Djide, M. N.; Amir, M. N.; Permana, A. D. Phenolic-Rich Green Tea Extract Increases the Antibacterial Activity of Amoxicillin against Staphylococcus Aureus by in Vitro and Ex Vivo Studies. *J. Pharm. Pharmacogn Res.* **2020**, *8* (6), 491−500.
(65) Visvalingam, J.; Palaniappan, K.; Holley, R. A. In Vitro Enhancement of Antibiotic Susceptibility of Drug Resistant Escherichia Coli by Cinnamaldehyde. *Food Control* **2017**, *79*, 288−291.

https://doi.org/10.1021/acsomega.4c01016
ACS Omega 2024, 9, 41157−41170